Ultrasonics Sonochemistry 79 (2021) 105782

Contents lists available at ScienceDirect

Ultrasonics Sonochemistry

journal homepage: www.elsevier.com/locate/ultson

Effect of cavitation bubble on the dispersion of magnetorheological polishing fluid under ultrasonic preparation

Ce Guo [a,b,*], Jing Liu [a], Xiuhong Li [a], Shengqiang Yang [a]

[a] Shanxi Key Laboratory of Precision Machining, College of Mechanical and Vehicle Engineering, Taiyuan University of Technology, 030024 Taiyuan, China
[b] Taiyuan Heavy Mechinery Group Co., LTD, 030024 Taiyuan, China

ARTICLE INFO

Keywords:
Ultrasonic dispersion
Cavitation
Magnetorheological polishing fluid
Bubble dynamics

ABSTRACT

In the ultrasonic dispersion process, the ultrasonic cavitation effect can seriously affect the dispersion efficiency of magnetorheological polishing fluid (MRPF), but the mechanism remains unclear now. Through considering the continuity equation and Vand viscosity equation of the suspension, a revised cavitation bubble dynamic model in the MRPF was developed and calculated. The effects of presence or absence of solid particles, the volume fraction of solid particles, and viscosity on the cavitation bubble motion characteristics in the MRPF were discussed. Settlement experiments of the MRPF under ultrasonic and mechanical dispersion were observed. Analysis of particle dispersion is made by trinocular biomicroscope and image processing of the microscopic morphology of the MRPF. The results show that the high volume fraction of carbonyl iron particle (CIP) will significantly weaken the cavitation effect, and the low volume fraction of green silicon carbide (GSC) has a negligible effect on the cavitation effect in the MRPF. When the liquid viscosity is greater than or equal to 0.1 Pa·s, it is inconvenient to produce micro-jets in the MRPF. The sedimentation rate of the MRPF prepared by ultrasonic dispersion is lower than mechanical dispersion when the volume fraction of CIP is between 1% and 25%. The dispersion ratio under ultrasonic dispersion is lower than that under mechanical dispersion. The experimental results fit the simulation well. It offers a theoretical basis for exploring the ultrasonic cavitation effect in the industrial application of the MRPF.

1. Introduction

Magnetorheological fluid (MRF) is an excellent, intelligent material, and its mechanical property can be regulated by the external magnetic field, which is widely used in nuclear magnetic resonance, targeting therapy, magnetic fluid seal, magnetorheological damping, and magnetorheological polishing, with the advantages of green, environmental protection and intelligent controllability[1–2]. The typical application of the MRF in the field of precision and ultra-precision polishing for high-performance parts is magnetorheological polishing fluid (MRPF) [3–4]. MRPF is a solid–liquid suspension composed of magnetic or non-magnetic solid particles, base solution, and a small number of additives. When different kinds of solid particles are mixed, they are easy to agglomerate and settle. The reason is perhaps that the density of solid particles is more than that of the base fluid[5]. Therefore, in the preparation and utilization of the MRPF, dispersion technology should be utilized to homogenize solid particles. However, due to the complexity of multiphase flow and a lack of micro understanding of granule dispersion for the MRPF, the dispersion mechanism of solid particles has become a challenging issue in magnetorheological polishing.

Traditional physical dispersion methods such as mechanical stirring with blades and ball milling are time-consuming, have low precision, and have poor controllability. It is difficult to disperse various solid particles uniformly in the base solution[6]. Ultrasonic dispersion uses its own physical and chemical effect in a liquid to disperse solid particles. As a certain intensity of ultrasonic wave passes through the liquid, the cavitation effect will occur. The cavitation effect can generate large numbers of oscillating bubbles. The oscillating bubbles may collapse near the solid particles and release micro-jets and shock waves, which will have a serious impact on the solid particle population[7–8]. It proves efficient for the dispersion of solid particles in suspension. However, present research on the ultrasonic dispersion of the MRPF focuses on its process regulation and still lacks a mechanism explanation for cavitation dispersion. For example, the dynamics of the generation,

* Corresponding author at: Shanxi Key Laboratory of Precision Machining, College of Mechanical and Vehicle Engineering, Taiyuan University of Technology, 030024 Taiyuan, China.
E-mail address: guoce1027@163.com (C. Guo).

https://doi.org/10.1016/j.ultsonch.2021.105782
Received 29 August 2021; Received in revised form 28 September 2021; Accepted 4 October 2021
Available online 9 October 2021

growth, and collapse of cavitation bubbles in the MRPF do not explain well.

The extent of the particle distribution of the MRPF is closely related to the dynamics characteristics of the cavitation bubble. The dynamic bubble model is used for describing the dynamic characteristics of the cavitation bubble. Rayleigh established the first inviscid and incompressible bubble dynamics model based on the Bernoulli equation[9]. Plesset et al. modified Rayleigh's equation by considering the liquid viscosity and surface tension to obtain the classical Rayleigh-Plesset model[10]. The Rayleigh-Plesset model can simulate the cavitation bubble dynamic process more accurately and efficiently, and it preserves the validity and manageability in the application of the bubble model. Afterward, lots of new models were provided by modifying the Rayleigh-Plesset equation, such as the Keller-Miksis model[11] and Gilmore model[12] considering the liquid compressibility, Flynn model[13] considering the thermodynamic characteristics of the gas inside the bubble, and others. In recent years, some scholars have begun to focus on the application of the bubble dynamics model in suspension, such as visco-elastic fluids[14], complex rheology fluids[15], and grinding fluid [16]. However, the present cavitation bubble model is mainly suitable for water solution or the liquid approximated as a water solution. There is a lack of research on the bubble model of solid–liquid suspension.

With the development of numerical technique, computational fluid dynamics, multi-physics coupling, and other numerical methods have been extensively used to simulate the acoustic fields and flow fields of the suspension [17–18]. In practice, however, these numerical calculation methods usually ignore the cavitation effect of the liquid due to the complex physical and chemical mechanism of cavitation bubbles. How to reveal the acoustic cavitation effect of the suspension has become a challenging issue in ultrasonic dispersion.

In the paper, we provide a revised Rayleigh-Plesset equation to analyze the mechanism of cavitation dispersion in the MRPF, considering the solid/liquid ratio of the suspension. The dynamic parameters affecting the motion and collapse of the cavitation bubble of the MRPF are discussed in detail. Sedimentation and dispersion experiments in the MRPF are used to verify the conclusion of the theoretic analysis. It will provide theoretical support for the ultrasonic preparation process of the MRPF.

2. Cavitation theory under the MRPF

2.1. Physical environment

General composition of the MRPF is shown in Table 1. The solid phase of the MRPF consists of carbonyl iron particle (CIP), green silicon carbide(GSC), and a small number of additives[19]. The CIP, as a magnetic-sensing particle, is the primary evoked factor of the high shear yield strength and rheological property of the MRPF. GSC is generally selected as the abrasive particles of the MRPF to grind or finish. CIP has a primary particle size of approx. 5 μm and GSC of approx. 40 μm. Additives play a crucial role in enhancing the surface activity of solid particles, such as carboxymethyl cellulose sodium, sodium hexametaphosphate, sodium nitrite, anhydrous sodium carbonate, and nano-silica. It can partly inhibit the agglomeration of solid particles in the MRPF and prevent the solid particles from settling. Unlike the solid phase, the liquid phase of the MRPF is mixed with deionized water and propanetriol, which are the main component of the MRPF.

Table 1
General composition of the MRPF.

Paremeters		Values	Volume fraction
Liquid phase	Deionized water	70 ml	60.99%
	Propanetriol	1 ml	
Solid Phase	Carbonyl iron particle	230 g	25.07%
	Green silicon carbide	30 g	8.12%
	Carboxymethyl cellulose sodium	0.33 g	5.89%
	Sodium hexametaphosphate	1.35 g	
	Sodium nitrite	0.2 g	
	Anhydrous sodium carbonate	0.4 g	
	Nano-silica	4.32 g	

Before preparation, various additives should be added to the deionized water sequentially and manually stirred simultaneously. After that, CIP and GSC are added to the mixture and mechanically stirred until there is no visible large agglomeration. Finally, the suspension is dispersed by ultrasonic treatment for 0.5 ~ 3 min. The ultrasonic wave and its cavitation effect can effectively enhance the dispersion rate of the solid particles in the suspension, shorten the preparation time of the MRPF and improve its preparation efficiency.

2.2. Cavitation bubble dynamic model

The MRPF is used in industrial applications where an external magnetic field is normally applied. Magnetic solid particles tend to converge and form a chain-like structure along the magnetic induction line under the magnetic field. Under the condition, the MRPF is a highly viscous semi-solid substance. However, in the preparation of the MRPF, the magnetic field is not applied externally, the solid particles in the MRPF should be uniformly dispersed in the base fluid and behave as a Newtonian fluid. Therefore, the cavitation bubble dynamic model discussed in this paper is suitable for the preparation of the MRPF under non-magnetic fields.

When an ultrasonic wave with a certain intensity passes through the MRPF, the cavitation effect occurs, and cavitation bubbles are produced. The cavitation bubble of the MRPF are assumed as follows: 1) the bubble remains spherical in the process of expansion and contraction, and the center of the bubble is fixed; 2) the gas in the bubble is ideal, and its isothermal and adiabatic processes are considered; 3) the solid–liquid mixed ratio is considered, and the suspension is an incompressible viscous flow; 4) the heat exchange, interfacial phase change, and chemical reaction are not considered. Then, according to the law of energy conservation of the cavitation process in a liquid, the Rayleigh-Plesset equation is introduced to reveal the cavitation effect as follows [20]

$$R\frac{\mathrm{d}^2\mathrm{R}}{\mathrm{dt}^2}+\frac{3}{2}\left(\frac{\mathrm{dR}}{\mathrm{dt}}\right)^2=\frac{p}{\rho}+\frac{R}{\rho c}\frac{\mathrm{d}}{\mathrm{dt}}\left(p_{\mathrm{g}}-\mathrm{p_A}\right) \tag{1}$$

$$p=p_{\mathrm{g}}+\mathrm{p_v}-\frac{2\sigma}{\mathrm{R}}-4\mu\frac{\dot{\mathrm{R}}}{\mathrm{R}}-\mathrm{p_0}-\mathrm{p_A} \tag{2}$$

where R is the instantaneous radius of the bubble, c is the sound velocity of the MRPF, ρ is the density of the MRPF, σ is the surface tension coefficient of the MRPF, μ is the viscosity coefficient of the MRPF, p_g is the pressure inside the bubble, p_v is the saturation vapor pressure inside the bubble, p_0 is the static pressure of the MRPF, $p_A = -p_a\sin(2\pi ft)$ is the external ultrasonic wave, p_a is the pressure amplitude of the ultrasonic wave, f is the ultrasonic frequency, and t is time.

The bubble content of the MRPF is assumed to be uniformly distributed. The dynamic process from bubble growth to compression is regarded as isothermal, while bubble compression and collapse is treated as adiabatic. Then, the pressure p_g inside the bubble of the MRPF can be expressed as follows [21–22]

$$p_{\mathrm{g}}=\begin{cases}\left(\mathrm{p_0}+\dfrac{2\sigma}{\mathrm{R_0}}-\mathrm{p_v}\right)\left(\dfrac{\mathrm{R_0}}{\mathrm{R}}\right)^3, & \mathrm{R_0}\leqslant\mathrm{R}\leqslant R_{max}\\ \left(\mathrm{p_0}+\dfrac{2\sigma}{\mathrm{R_0}}-\mathrm{p_v}\right)\left(\dfrac{\mathrm{R_0^3}}{\mathrm{R^3}-\mathrm{a^3}}\right)^{\gamma}, & R_{min}\leqslant\mathrm{R}\leqslant\mathrm{R_0}\end{cases} \tag{3}$$

where R_0 is the initial radius of the bubble, R_{min} is the minimum radius of the bubble, R_{max} is the maximum radius of the bubble, γ is the adiabatic gas index, and a is the van der Waals radius ($R_0/a = 8.54$).

From the aspect of fluid–structure interaction mechanics, the MRPF is deemed to be a two-phase flow consisting of various solid particles and

a base liquid. In the process of ultrasonic dispersion, the solid particles can be rapidly and uniformly dispersed in the base liquid under the cavitation effect occurring in the suspension. As the solid particle size is in the micron or nanometer scale, the solid particles and the liquid medium can move at the same speed. Because the homogeneous mixture approach is generally used to describe the liquid–solid two-phase flow under the action of cavitation[23]. The liquid–solid phases are assumed to be sufficiently well mixed and the disperse particle size are sufficiently small thereby ignoring any significant relative motion. In this situation, the interface of solid–liquid two-phase flow is strongly coupled. Thus, two-phase flow of solid–liquid can be assumed as unidirectional flow motion. For this reason, the equation of continuity of the mixture can be introduced as[24]

$$\frac{\partial \rho}{\partial t} + \nabla(\rho u) = 0 \tag{4}$$

$$\rho = \sum_k \alpha_k \rho_k \tag{5}$$

where u is the flow rate of the mixture, k is the type of phase, α_k is the volume fraction, and ρ_k is the density of a phase.

Before cavitation, those trace gas or vapor nuclei in the base solution can be ignored. Thus, the density ρ of the MRPF can be expressed as

$$\rho = \alpha_p \rho_p + \alpha_l \rho_l \tag{6}$$

where α_p and α_l are the volume fraction occupied by the solid particles and the base solution, and ρ_p and ρ_l are the density of that, respectively.

The viscosity of the MRPF is related to the type of solid particles, particle geometry, particle concentration, and the ratio of the base solution. However, it is the volume fraction of solid particles that plays a decisive role in viscosity. For the diluted suspension, Einstein gives the following formula for viscosity[25]

$$\mu = \mu_0(1 + k''\alpha_p) \tag{7}$$

where μ_0 is the viscosity of the base solution and k" is the constant of particle shape, for spherical particles, k"=2.5.

However, Eq. (7) is only applicable to the case where the volume fraction of solid particles does not exceed 2% and does not meet the requirements for the preparation of the MRPF. To solve the problem, Vand proposed a revised equation for the viscosity of a high volume fraction of solid particles [26]

$$\mu = \mu_0 e^{k''\alpha_p/(1-a'\alpha_p)} \tag{8}$$

where, a' is another constant of particle shape, for spherical particles, $a' = 39/64 = 0.609$. Considering the need for the viscosity in the preparation of the MRPF, the Vand viscosity equation is introduced to describe the viscosity of the MRPF.

Integrating Eqs. (2), (3), (6), and (8), a revised cavitation bubble dynamic model of Eq. (1) is established to describe the cavitation effect in the MRPF under ultrasound dispersion. Furthermore, Eq. (1) can be solved numerically using the fourth-order Runge-Kutta method. The initial conditions are as follows: at $t = 0$, $R = R0$, $dR/dt = 0$. The physical parameters of the MRPF are shown in Table 1, where $\rho_{CIP} = 7.89 \times 10^3$ kg/m3, $\rho_{GSC} = 3.17 \times 10^3$ kg/m3, $\rho_{additive} = 1.22 \times 10^3$ kg/m^3, $\rho_l = 1.0 \times 10^3$ kg/m^3, and the other parameters are as follows: $c = 1481$ m/s, $\gamma = 4/3$, $p_v \approx 0$ Pa, $p_0 = 1.013 \times 105$ Pa, $\sigma = 7.28 \times 10^{-2}$N/m, $\mu_0 = 1.005 \times 10^{-3}$ Pa·s.

During ultrasonic dispersion, the schematic diagram of the cavitation dispersion mechanism is described in Fig. 1. The cavitation bubble under ultrasonic wave presents a series of dynamical behaviors such as expansion, shrink and collapse. As the collapse of the cavitation bubble occurs near a solid wall, a micro-jet with a high velocity can develop through the center of the bubble towards the wall[27]. The micro-jet plays a major role in surface treatment and aggregates breakup [28–29]. The aggregates are broken and become smaller during the cavitation micro-jet dispersion, and the smaller aggregates are more easily to be dispersed in the base solution, which is meaningful to increase the dispersion efficiency of the MRPF. Jet velocity is the principal characteristic of cavitation micro-jet. It mainly depends on the cavitation bubble dynamics model in specific fluid environments[30]. Although ultrasonic cavitation have been studied for many years, there are still no uniform conclusions for micro-jets due to various influencing factors[31–32]. Therefore, in the paper, the revised Rayleigh-Plesset equation is used to deal with the motion characteristics of the cavitation bubble and the micro-jet it generates during collapse in the MRPF, which is of great significance for further exploring the ultrasonic dispersion of the MRPF.

2.3. Stability of the MRPF

2.3.1. Sedimentation ratio

In industrial applications, improving the stability of the MRPF is the most urgent problem, and rheological property is the secondary issue. When the MRPF remains stationary for some time, the denser solid particles tend to settle, and a continuous phase will occur on the top of the suspension. The height of supernatant liquid and total suspension can be recorded at the specified time. A percentage value of the volume of supernatant liquid and volume of total suspension can be defined as sedimentation ratio as follows[33–34]

$$\text{Sedimentation ratio} = \frac{\text{Volume of supernatant liquid}}{\text{Volume of total suspension}} \times 100\% \tag{9}$$

where the volume of supernatant liquid and suspension can be calculated by multiplying their height by the cross-section area.

2.3.2. Dispersion ratio

In order to characterize the dispersed solid particles and their agglomeration under ultrasonic cavitation, the microstructure of the MRPF was characterized using a DYS-107 trinocular biomicroscope. A

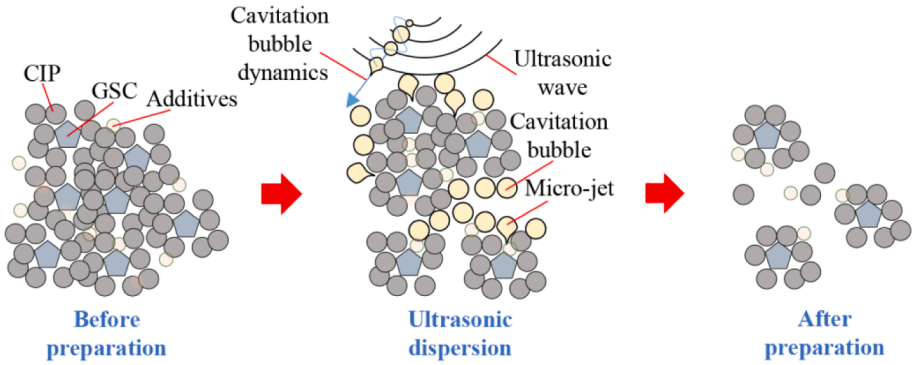

Fig. 1. The schematic diagram of the cavitation dispersion mechanism.

small amount of the MRPF is aspirated onto a slide from the resting suspension for observation. The dispersion state of the particles in the MRPF is the foremost consideration. The size distribution and particle shape are not the focus of the analysis. Pre-processing such as image binarization and normalization of the micrograph should be done for simplification. Subsequently, a series of gray images are obtained to study the dispersion stability of the MRPF. A dispersion ratio of the MRPF is defined and calculated as the proportion of black pixel points to the whole image of the gray image as follows

$$\text{Dispersion ratio} = \frac{\text{Black pixel points of the gray image}}{\text{Whole image points of the gray image}} \times 100\% \quad (10)$$

The dispersion ratio can approximate the percentage of the solid particles in the liquid phase. A large dispersion ratio means a weak particle dispersion, and a small dispersion ratio means a high particle dispersion.

3. Results and discussion

3.1. Effect of presence or absence of solid particles

Numerical simulations are carried out for revealing the cavitation bubble dynamics of ultrasonic dispersion preparation in the MRPF, with an ultrasonic frequency of 20 kHz, ultrasonic pressure amplitude of 0.3 MPa, and the initial radius of the bubble of 10 μm. Fig. 2 shows the effect of the presence or absence of solid particles on the motion characteristics of the cavitation bubble in the MRPF. In the absence of solid particles, the volume fraction of solid particles in Eq. (6) can be ignored.

Fig. 2(a) describes the dimensionless radius of the bubble versus time. From Fig. 2(a), it can be seen that the bubble of the MRPF undergoes the dynamic process of growth, expansion, compression, and collapse under one acoustic cycle. However, the presence or absence of solid particles in the base solution has noticeable influence on the bubble motion. After the addition of solid particles in the base solution, the bubble expansion is tremendously reduced, and the collapse time of the bubble is also prolonged. It indicates that the addition of solid particles significantly weakens the original cavitation effect of the MRPF.

Fig. 2(b) shows the variation of bubble velocity with dimensionless radius, which presents the periodic nonlinear vibration process in the bubble compression phase. It can be described that the limit rings appear on the phase plane regardless of whether the suspension contains solid particles or not. When solid particles are added to the base liquid solution, the limit ring starts to become smaller. It is due to the decrease of the cavitation effect of the MRPF. From Fig. 2(b), when there are no solid particles of the suspension, the bubble can be compressed to a minimum of 0.1259 times of the initial radius and then generates a collapse velocity ($v_{collapse}$) of 3.791 × 10^4m/s, where $v_{collapse}$=|max(dR/dt)|. However, after consideration of solid particles, the bubble can be compressed to a minimum of 0.1282 times of the initial radius and releases a collapse velocity of 1.025 × 10^4m/s. It also indicates that the cavitation bubble is less compressed, and the impact velocity released by bubble collapse is significantly weaker when solid particles are added to the base solution. Research has found that the bubble can generate the micro-jet near a rigid interface, where the bubble collapse velocity is

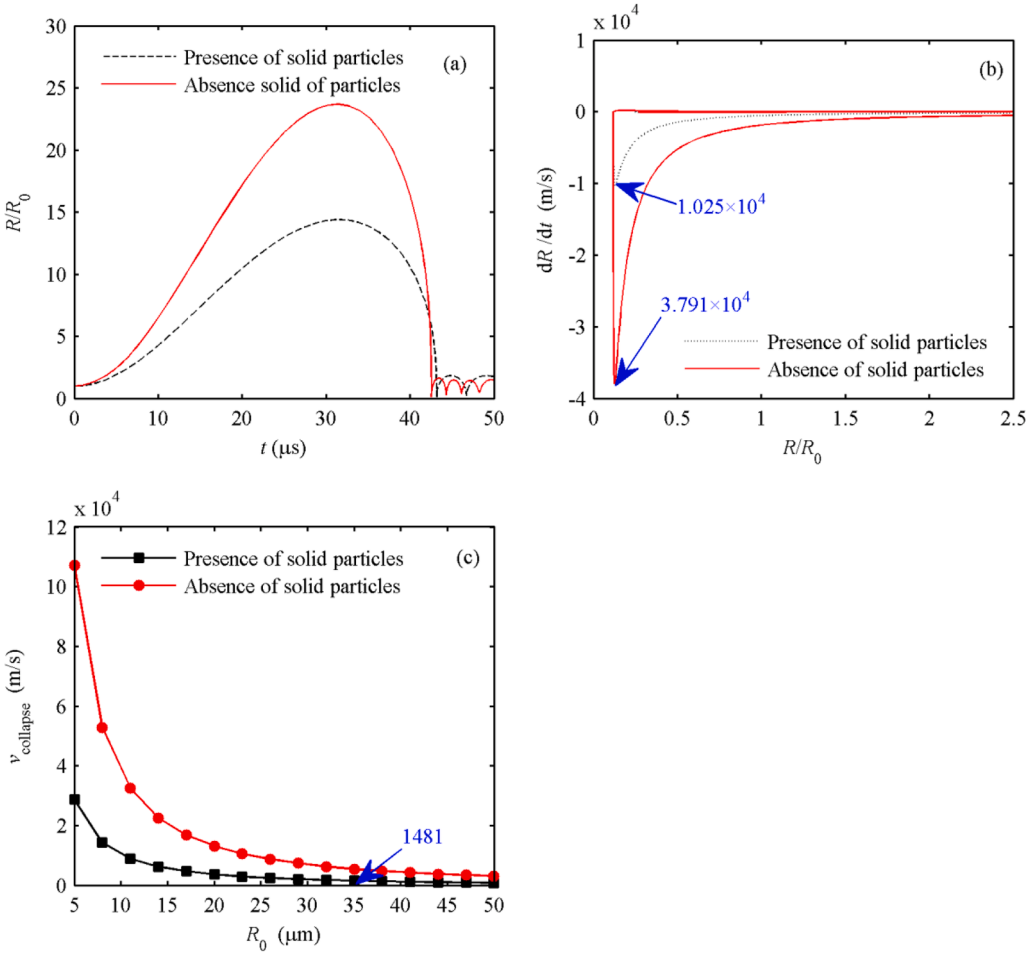

Fig. 2. The effect of presence or absence of solid particles on the motion characteristics of the cavitation bubble in the MRPF. (a) Dimensionless radius of the bubble versus time; (b) Bubble velocity with dimensionless radius; (c) Bubble collapse velocity with initial bubble radius.

greater than the sound velocity of the fluid[35]. Because the bubble collapse velocity of work is one order of magnitude higher than the sound velocity of the MRPF($c \approx 1481$ m/s), the micro-jet near the solid particles can be produced. The micro-jet will have a remarkable impact and dispersion on solid particles, which can be treated as one of the micro-mechanisms for revealing the uniform dispersion of solid particles.

Fig. 2(c) shows the variation of the bubble collapse velocity versus the initial bubble radius of 5–50 μm. The bubble collapse velocity is reduced with the increase of the initial bubble radius. It is because that the large bubble is compressed in the positive phase of ultrasound, but it does not expand to the maximum in the subsequent negative phase of ultrasound. For various initial bubble radii of the MRPF, the bubble collapse velocity is all lower than that without the addition of solid particles. Thus, for the MRPF with the addition of various solid particles, the large bubble will further weaken the micro stirring ability for solid particles.

Moreover, in Fig. 2(c), when the initial bubble radius is 35 μm, the bubble collapse velocity of the base solution with solid particles is 1481 m/s, which is just equal to the sound velocity of the MRPF. With increasing the initial bubble radius, the collapse velocity of the bubble will be further reduced, where the micro-jet will not continue to be produced in theory. Therefore, during the preparation of the MRPF, the larger bubble will not produce micro-jets in the vicinity of solid particles, which will lead to a weaker or even no dispersion effect of cavitation bubbles on solid particles.

3.2. *Effect of the volume fraction of solid particles*

Fig. 3 shows the effect of the volume fraction of solid particles on cavitation bubble motion characteristics in the MRPF. The solid particles with high volume fraction in the MRPF, such as CIP and GSC, are discussed in detail. Fig. 3(a) presents the variation of the bubble radius under various volume fractions of CIP. In Fig. 3(a), it can be observed that for CIP of the MRPF, with increasing the volume fraction of CIP, the expansion amplitude of the cavitation bubble is decreased, and the collapse time of the bubble is shortened. Jun demonstrates that solid particles disturb the shear flow of suspension and then increase the shear viscosity[36]. Thus, the heavy volume fraction of solid particles adding in the based fluid will result in high shear viscosity. From Fig. 3(a), high liquid viscosity leads to the slow bubble growth. When the volume fraction of CIP exceeds 25%, the viscosity of the MRPF will increase linearly, and then the growth of the cavitation bubble will be more difficult.

Fig. 3(b) presents the variation of the bubble radius under various volume fractions of GSC. From Fig. 3(b), it can be observed that for the relatively low volume fraction of GSC of the MRPF, the expansion amplitude of the cavitation bubble slightly increases with the increase of volume fraction of GSC. In contrast, the collapse time of the bubble has little change. It indicates that the ultrasonic cavitation effect of the MRPF can be seriously affected by the high volume fraction of solid particles and is scarcely influenced by the low volume fraction of solid particles.

Fig. 3(c) shows the bubble collapse velocity with the volume fraction

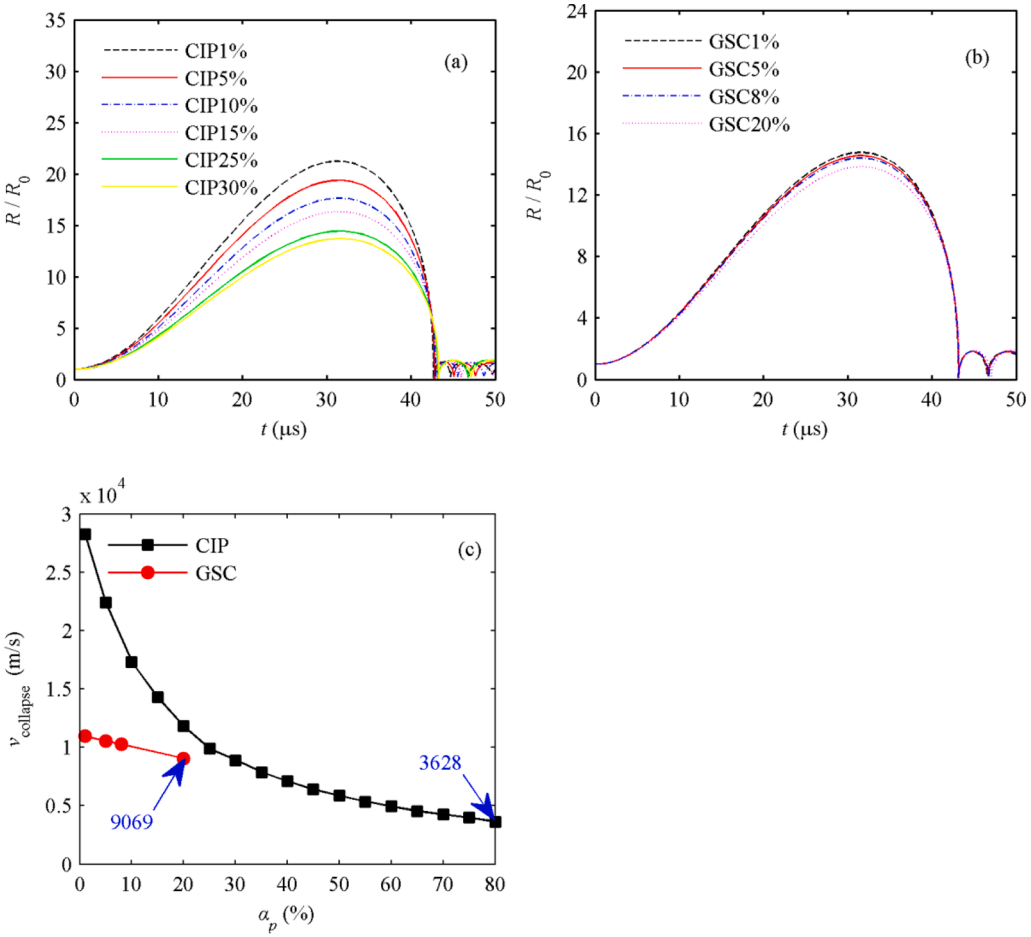

Fig. 3. Effect of the volume fraction of solid particles on cavitation bubble motion characteristics in the MRPF. (a) Variation of the bubble radius under various volume fractions of CIP; (b) Variation of the bubble radius under various volume fractions of GSC;(c) Bubble collapse velocity with the volume fraction of CIP and GSC.

of CIP and GSC. As can be seen in Fig. 3(c), the bubble collapse velocity significantly decreases with increasing the volume fraction of CIP. At the same time, it reduces slightly with increasing the concentration of GSC. Compared with GSC, CIP has a greater effect on the cavitation effect. Thus, the ultrasonic cavitation effect can be regulated through varying the volume fraction of CIP. The cavitation bubble collapse velocity will fall to a minimum of 3628 m/s, with the volume fraction of CIP of 80%, while it will decrease to a minimum of 9069 m/s, with the volume fraction of GSC of 20%. It demonstrates that the bubble collapse velocity under varying the volume fraction of CIP or GSC is always higher than the sound velocity of the MRPF. Then the micro-jet can be produced near the solid particles. Nevertheless, it is not competent to control the formation of micro-jets through varying the volume fraction of solid particles due to the limited adjustment range of micro-jets.

3.3. The effect of viscosity

Fig. 4 shows the effect of the viscosity on the motion characteristics of the cavitation bubble in the MRPF. Fig. 4(a) presents the variation of the bubble radius under various viscosity. From Fig. 4(a), it can be seen that the expansion amplitude of the cavitation bubble is decreased, and the collapse time is shortened with the increase of viscosity. It indicates that the viscosity of the MRPF mainly plays an inhibitory role in the cavitation bubble movement. Nazari-Mahroo proposed that the liquid viscosity affects the bubble dynamics in the collapse phase, particularly at high ultrasonic amplitude and high viscosity [37]. Thus, for the high viscosity of the MRPF, there is a significant inhibitory effect on cavitation bubbles, and it can not be suitable to use ultrasonic dispersion to prepare a suspension individually.

The variation of the bubble collapse velocity with viscosity is given in Fig. 4(b), where the dotted line is the location of the sound velocity of the MRPF. From Fig. 4(b), it can be seen that when the viscosity is low (<0.1 Pa·s), the bubble collapse velocity decreases linearly as the increase of viscosity. The bubble collapse velocity is reduced to 1467 m/s with the viscosity of 0.1 Pa·s, which is slightly lower than the sound velocity of the MRPF of 1481 m/s. So, in this case, it is difficult for the cavitation bubble to generate micro-jets around the solid particles. When the viscosity of the MRPF continues to increase (≥0.1 Pa·s), the collapse velocity of the bubble is sharply reduced. For the viscosity of 0.5 Pa·s, the bubble collapse velocity is 1.1 m/s, which is much lower than the sound velocity of the MRPF. It is clear that for the high viscosity of the MRPF, the cavitation effect is so weak that the cavitation bubble does not produce micro-jets on solid particles. Luo also proved that the viscosity of the liquid medium would suppress the formation of the micro-jet, as well as delays the velocity of the micro-jet flowing toward the wall surface[38].

During the MRPF preparation, the addition of lots of non-uniform solid particles will increase the viscosity of the fluid inevitably. Moreover, the mechanical stirring for a long time will also lead to a sharp increase in the viscosity of the suspension. Therefore, ultrasonic dispersion should be used when the liquid viscosity is not greater than 0.1 Pa·s. For high viscosity, the cavitation effect induced by ultrasonic waves in the MRPF is inapparent, and the micro-jet near solid particles will not arise, so it should not continue to use ultrasonic dispersion to prepare the MRPF.

3.4. Sedimentation stability of the MRPF

The settling property of the suspension is an important index to evaluate its performance, and it can indirectly describe the dispersion of the particles [39]. In order to evaluate the ultrasonic cavitation on the dispersion effect of the MRPF, sediment experiments were carried out. The schematic of the experimental apparatus of ultrasonic and mechanical dispersion is shown in Fig. 5. The CIP of solid particles with a strong influence on ultrasonic cavitation was selected for sediment experiments. Various volume fractions of CIP in the MRPF are obtained in Table 2. The experimental conditions of ultrasonic and mechanical dispersion are shown in Table 3. The sedimentation rate was examined after the MRPF was left to stand for 8 h.

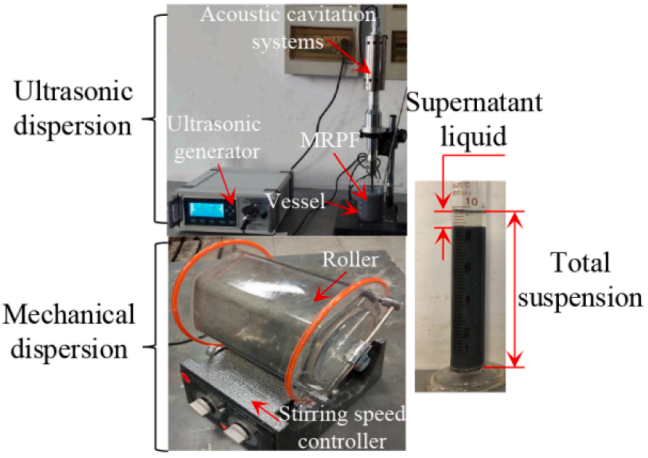

Fig. 5. The schematic of experimental apparatus of ultrasonic and mechanical dispersion.

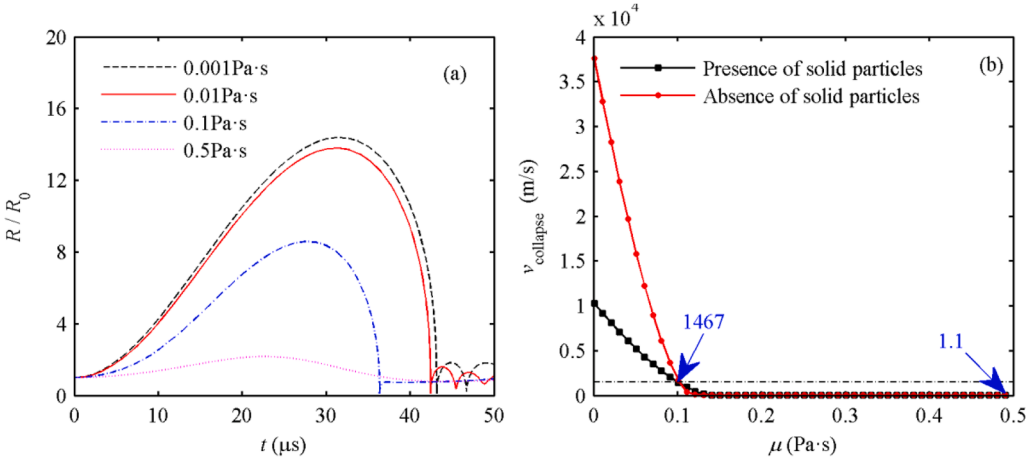

Fig. 4. Effect of the viscosity on the motion characteristics of the cavitation bubble in the MRPF. (a) Variation of the bubble radius under various viscosity; (b) Bubble collapse velocity with viscosity.

Table 2
Various volume fractions of CIP in the MRPF.

Composition	1%CIP	5%CIP	10%CIP	15%CIP	25%CIP	30%CIP
Deionized water	94.17%	88.91%	82.37%	75.76%	62.65%	56.04%
Propanetriol	1.34%	1.26%	1.17%	1.08%	0.89%	0.8%
GSC	0.33%	1.67%	3.3%	5%	8.3%	10%
Carboxymethyl cellulose sodium	0.48%	0.48%	0.48%	0.48%	0.48%	0.48%
Sodium hexametaphosphate	0.80%	0.80%	0.80%	0.80%	0.80%	0.80%
Sodium nitrite	0.18%	0.18%	0.18%	0.18%	0.18%	0.18%
Anhydrous sodium carbonate	0.14%	0.14%	0.14%	0.14%	0.14%	0.14%
Nano-silica	1.56%	1.56%	1.56%	1.56%	1.56%	1.56%

Table 3
Experimental conditions.

Parameters	Values
Ultrasonic power	500 W
Ultrasonic frequency	20 kHz
Ultrasonic time	30 s
Mechanical stirring speed	200r/min
Mechanical stirring time	3 h

The comparison of the sedimentation rates of the MRPF prepared under ultrasonic and mechanical dispersion is shown in Fig. 6. It can be seen that the sedimentation rate of the MRPF prepared by ultrasonic dispersion is lower than mechanical dispersion when the volume fraction of CIP is between 1% and 25%. It is because mechanical dispersion mainly uses the high-speed rotation of the medium to generate turbulent motion for dispersing the solid particle cluster. The maximum stirring speed of the suspension can be simplified as $v \approx r\omega = 2\pi nr$, where r is the stirring radius and n is the stirring speed. When $n = 200$r/min and $r = 200$ mm, $v = 251.2$ m/s. It can be seen that the stirring speed generated by mechanical dispersion on solid particles is much lower than that of ultrasonic dispersion(see Fig. 2(c), 3(c), and 4(b)). During ultrasonic dispersion, solid particles are affected by ultrasonic wave-induced cavitation field and bubble dynamics. The ultrasonic cavitation field will produce the flow fluctuations and macro stirring effect on the MRPF. Besides, at the micro-level, the micro-jets generated by the collapsing bubbles will have a distinct impact on solid particles. Thus, it is not easy to cause solid particles to coalesce and settle due to the above effects.

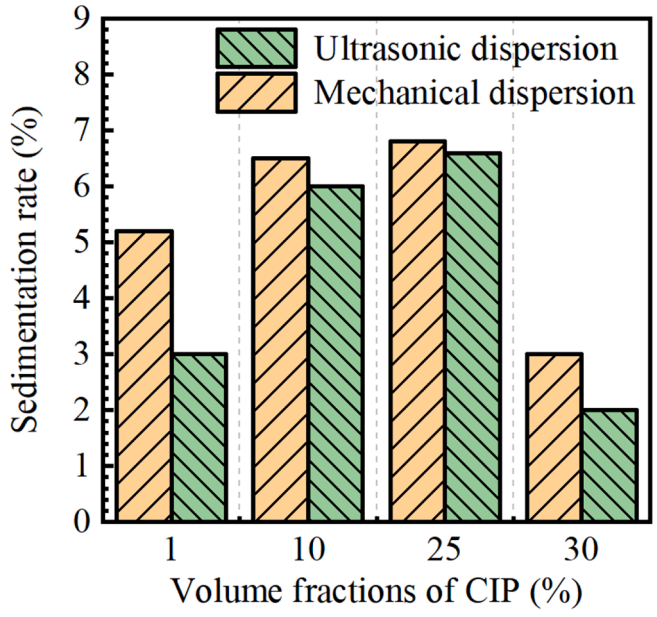

Fig. 6. The comparison of the sedimentation rates of the MRPF prepared under ultrasonic and mechanical dispersion.

Moreover, the sedimentation rate of the MRPF increases with the increase of the concentration of CIP when the volume fraction of CIP is between 1% and 25% in Fig. 6. The reason can be drawn from Fig. 3(a) and (c), as the volume fraction of CIP increases, the growth of the cavitation bubble becomes difficult, and the micro-jet velocity near the solid particles is decreasing accordingly. In other words, the effect of the motion characteristics of the cavitation bubble on the MRPF is weakened. Thus, the probability of aggregation of solid particles is increased, and they are easier to agglomerate and settle. There is also noted that the sedimentation rate at CIP volume fraction of 30% is lower than other volume fractions in the MRPF. For the high volume fraction of CIP, the MRPF is semi-solid and the viscosity of the MRPF will increase linearly. From Fig. 4(a) and (b), for the high viscosity of the MRPF, the cavitation effect induced by ultrasonic waves in the MRPF is inapparent, and the micro-jet near solid particles can not arise. Even if the settlement of the MRPF does not become visible, the rheology is becoming weaker under the magnetic field, so it is not suitable for the preparation of the MRPF.

3.5. Dispersion stability of the MRPF

For further highlight the ultrasonic cavitation effect of the MRPF, the microscopic morphology of the MRPF was tested by the trinocular biomicroscope. The measurement time is 24 h after the MRPF has been left to stand. The purpose of this is to allow the trace gas in the MRPF to evaporate completely so that the suspension can be considered to preserve the liquid and solid phases only. For comparison, the same scale was chosen for all microscopic images in the study. The magnification of each image is 40x. Fig. 7 shows the microstructure of the MRPF for various volume fractions of CIP under ultrasonic dispersion. As is shown in Fig. 7, it is found that various solid particles have been uniformly dispersed in the base solution after the MRPF is prepared. However, with the variation of the volume fraction of CIP, the particle distribution is also uneven. The probability of particle agglomeration increases with the increment of volume fraction of CIP, which tends to lead to instability of the MRPF.

Fig. 8 presents gray images to the micrograph of the MRPF for various volume fractions of CIP under ultrasonic dispersion. The black pixel points describe the particle phase, and the white zone is the liquid phase. The grayscale threshold is used to control the black and white ratio. For each grayscale map, the grayscale threshold keeps the same. The grayscale threshold is set at 0.5, which is a middle value. Afterward, the dispersion ratio of the MRPF is calculated and examined.

For comparison with ultrasonic dispersion, the microstructure and their gray images under mechanical dispersion are given in Figs. 9 and 10. It can be seen that under mechanical dispersion, the solid particles in the MRPF are easy together and form agglomerates. As the volume fractions of CIP increase, the probability of forming agglomerates by mechanical dispersion becomes higher and higher.

Fig. 11 depicts the dispersion ratio of the MRPF versus volume fractions of CIP. As can be observed in Fig. 11, the higher volume fraction of CIP yields a higher dispersion ratio. The dispersion ratio under ultrasonic dispersion is less than that under mechanical dispersion. Under the same conditions, ultrasonic dispersion get a better

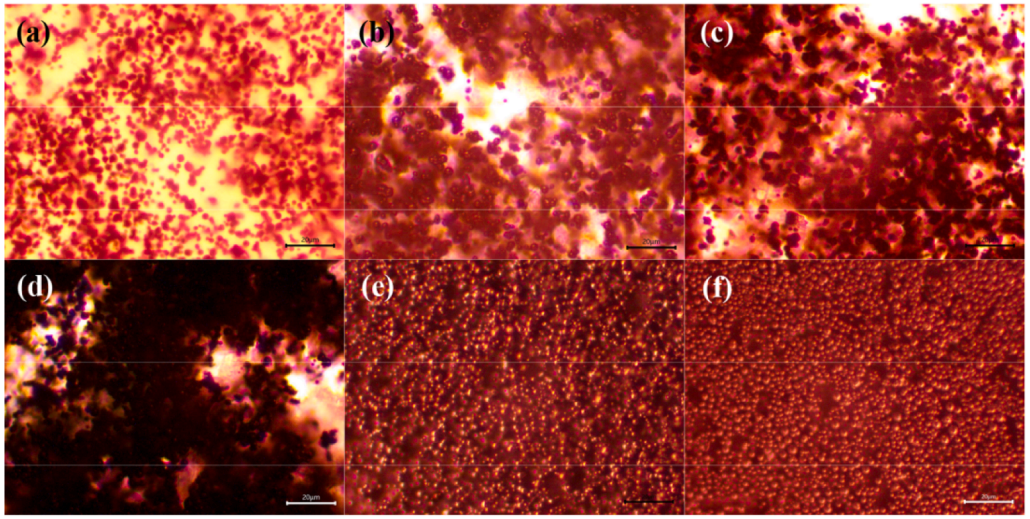

Fig. 7. Microstructure of the MRPF for various volume fractions of CIP under ultrasonic dispersion. (a)1%; (b)5%; (c)10%; (d)15%; (e)25%; (f)30%.

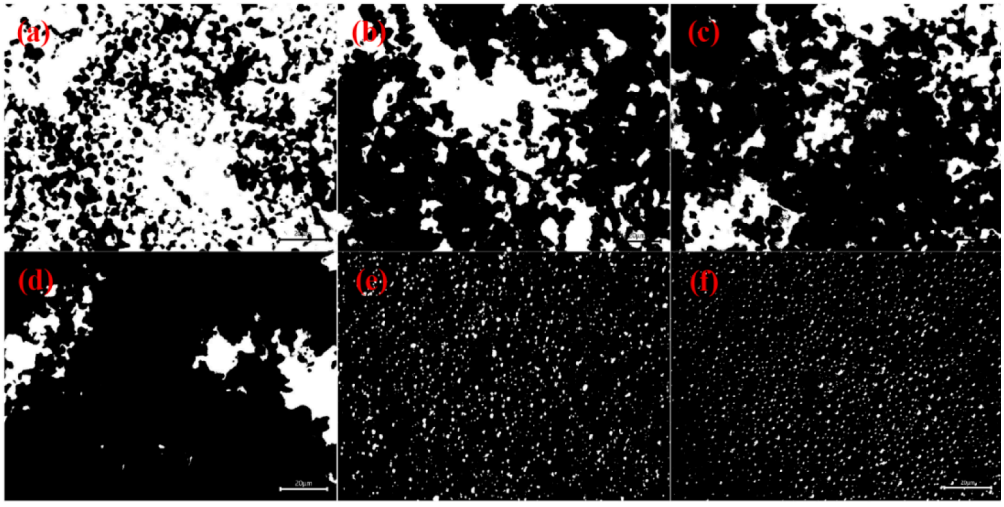

Fig. 8. Gray images to the microstructure of the MRPF for various volume fractions of CIP under ultrasonic dispersion. (a)1%; (b)5%; (c)10%; (d)15%; (e)25%; (f)30%.

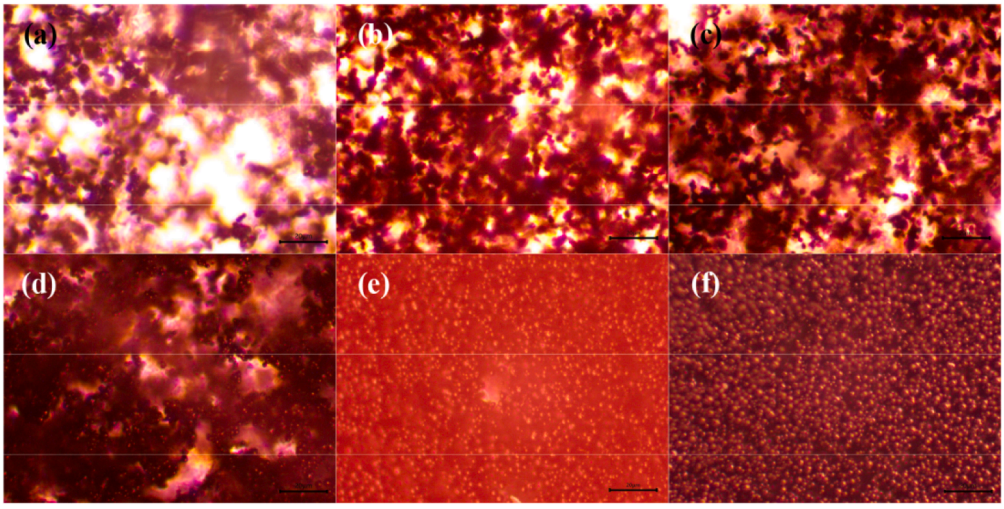

Fig. 9. Microstructure of the MRPF for various volume fractions of CIP under mechanical dispersion. (a)1%; (b)5%; (c)10%; (d)15%; (e)25%; (f)30%.

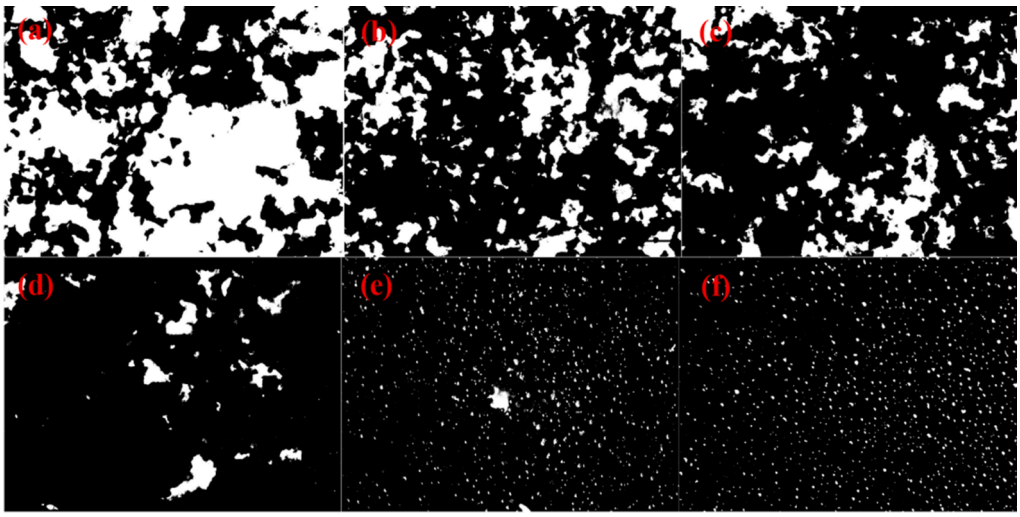

Fig. 10. Gray images to the microstructure of the MRPF for various volume fractions of CIP under mechanical dispersion. (a)1%; (b)5%; (c)10%; (d)15%; (e)25%; (f)30%.

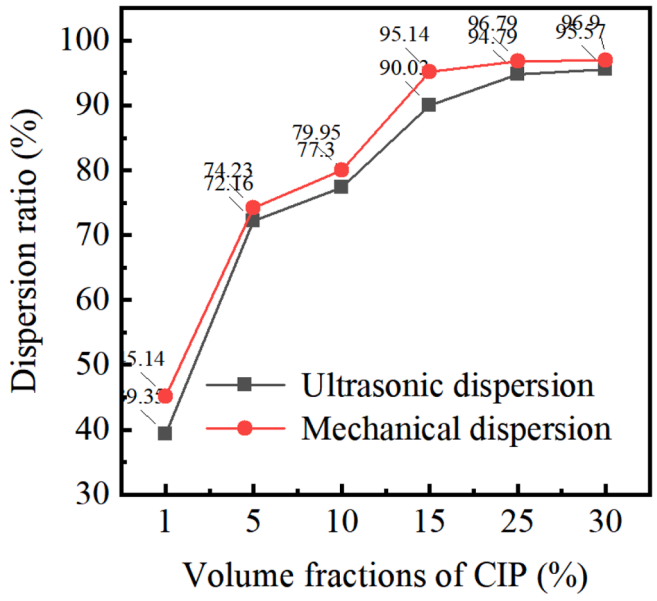

Fig. 11. Dispersion ratio of the MRPF versus volume fractions of CIP.

dispersion effect for the MRPF. From Fig. 2(a) and Fig. 3(a), ultrasound wave can produce the cavitation bubble in the MRPF containing solid particles with various volume fractions. When cavitation bubbles collapse near solid particles they also produce micro-jets to impact and disperse the MRPF, as shown in Fig. 2(c) and Fig. 3(c). However, it also indicates that the dense solid particles are less likely to be dispersed under ultrasonic and mechanical dispersion. For ultrasonic dispersion, the higher volume fraction of CIP will inhibit the bubble growth and reduces the micro-jet velocity, as described in Fig. 3(a) and (c). Further, it increases the viscosity of the MRPF and then significantly weakens the cavitation effect of the MRPF, as shown in Fig. 4(a) and (b). Nonetheless, the relatively weak micro-jets are still able to produce dispersion of solid particles. This is even worse for mechanical dispersion. In the process of mechanical dispersion, there are almost no active cavitation bubbles and micro-jets generated near the solid particles, resulting in solid particles coalescing more readily, which fits the previous simulation results very well.

Based on the theory of Derjaguin-Landau-Verwey-Overbeek, during ultrasonic dispersion, the dispersing or aggregation of particles were determined by the energy relations [40–41], as follow

$$E_a = E_u + E_c + E_s \tag{11}$$

where, E_a is the energy holding particles together, which is caused by Van der Waals'force. The other three energy acting on solid particles is used to destroy aggregates: E_u is the energy of ultrasonic wave propagation, E_c is the energy of collision between aggregates, and E_s is the energy of fluid shearing the particle aggregates.

When the energy of destroying aggregates is greater than the energy holding particles together, the aggregated particles can be dispersed. Thus, the energy of destroying aggregates needs to be as large as possible for the uniform dispersion of the MRPF.

In Eq. (11), E_c and E_s are associated with particle size, liquid properties and the flow rate of the liquid caused by agitation. Those factors are both considered in ultrasonic and mechanical dispersion.

However, in the ultrasonic dispersion, if we only consider the velocity v_m of a solid particle originated from the ultrasonic wave transmission in suspension, the kinetic energy can be presented as

$$E_u = \frac{1}{2} m_p v_m^2 \tag{12}$$

where, m_p is the mass of a solid particle.

In the study, the velocity v_c caused by the micro-jet from cavitation bubble collapse is included, and then the Eq.(12) can be rewritten as

$$E_u = \frac{1}{2} m_p (v_m + v_c)^2 \tag{13}$$

The value of the velocity v_m is in order of a few meters per second, but that of the velocity v_c is in the order of a few hundred meters per second [42–43]. The values of v_c may be approximated as two orders of magnitude higher than that of v_m. Thus, micro-jets will produce greater energy of destroying aggregates for solid particles, but the phenomenon is ignored in preparation of the MRPF process. We hold that the ultrasonic cavitation induced micro-jets are the microscopic reason that ultrasonic dispersion is superior to mechanical dispersion. Furthermore, the process parameters that can generate micro-jets need to be precise control in the MRPF process.

In summary, the paper explores the ultrasonic cavitation effect in the preparation of the MRPF from the bubble motion and the micro-jet of view. According to the conservation of energy during the motion of solid particles in the MRPF, the kinetic energy of solid particles will be converted into potential energy of dispersed motion of solid particles. Thus, the presence of the micro-jet is essential for the MRPF dispersion. In a

solid–liquid system, micro-jets may cause erosion and pitting on solid surface, removal of non-reactive coating, and particle fracture, as described in [44]. These factors will continue to be improved in future studies. The revised bubble dynamic model can be used to better explain the experimental results in the MRPF. There also have been limitations in the model at a 30% volume fraction of CIP. However, it does not affect the analysis and evaluation of the proposed bubble model for the common preparation of the MRPF.

4. Conclusion

Ultrasonic cavitation theory has been successfully introduced to reveal the dispersion mechanism of the MRPF. We presented a revised cavitation bubble dynamic model by considering the mixture continuity equation and Vand viscosity equation of the MRPF. The effects of three factors(presence or absence of solid particles, volume fraction of solid particles, and viscosity) on the cavitation bubble motion characteristics in the MRPF were dealt within detail. The sedimentation ratio and dispersion ratio were employed to evaluate the effect of ultrasonic cavitation on the MRPF dispersion. The following conclusions can be drawn from the study:

(1) After adding solid particles into the MRPF, the original cavitation effect of the suspension will be significantly weakened. The high volume fraction of CIP will significantly weaken the cavitation effect of the MRPF, and a lower volume fraction of GSC has little effect in the cavitation effect of the MRPF. The viscosity of the MRPF plays an inhibiting role on the cavitation effect of the MRPF. When the viscosity of the MRPF is greater than or equal to 0.1 Pa·s, it is difficult for the MRPF to produce micro-jets.
(2) The sedimentation rate of the MRPF prepared by ultrasonic dispersion is lower than mechanical dispersion when the volume fraction of CIP is between 1% and 25%. The dispersion ratio under ultrasonic dispersion is lower than that under mechanical dispersion. The experimental results can be interpreted in terms of cavitation bubble dynamics and the micro-jets they generate.

The model described in the paper shows good applicability in the volume fraction of CIP at 1%-25% and can be used for the theoretical analysis of cavitation effect in suspension such as magnetorheological polishing fluids, magnetorheological fluid and magnetic liquid.

CRediT authorship contribution statement

Ce Guo: Conceptualization, Methodology, Formal analysis, Validation, Funding acquisition, Writing – review & editing. **Jing Liu:** Software, Data curation, Writing – original draft. **Xiuhong Li:** Resources, Visualization. **Shengqiang Yang:** Supervision, Project administration.

Declaration of Competing Interest

The authors declare that they have no known competing financial interests or personal relationships that could have appeared to influence the work reported in this paper.

Acknowledgment

This work was supported by the National Natural Science Foundation of China (No. 51975399 and 52075362), the project funded by the Postdoctoral research Foundation of China(No. 2020M670712) and the National Science Foundation of Shanxi Province of China(No. 201901D211016).

References

[1] A.H. Dorosti, M. Ghatee, M. Norouzi, Preparation and characterization of water-based magnetorheological fluid using wormlike surfactant micelles, J. Magn. Magn. Mater. 498 (2020), 166193, https://doi.org/10.1016/j.jmmm.2019.166193.
[2] H. Prajapati, J. Shahanand, H. Nimkar, A. Lakdawala, Methods for sedimentation study of magnetorheological fluids, Mater. Today 28 (2020) 40–44, https://doi.org/10.1016/j.matpr.2020.01.138.
[3] A. Barman, M. Das, Nano-finishing of bio-titanium alloy to generate different surface morphologies by changing magnetorheological polishing fluid compositions, Precis. Eng. 51 (2018) 145–152, https://doi.org/10.1016/j.precisioneng.2017.08.003.
[4] J.H. Xu J.Y. Li P.Z. Zhu B.Z. Li C.Y. Zhao Coarse-grained molecular dynamics simulations of particle behaviors in magnetorheological polishing fluid Comp. Mater. Sci. 163 2019 /j.commatsci.2019.03.023. 68 81 https://doi.org/10.1016.
[5] P. Zhang, Y.Z. Dong, H.J. Choi, C.-H. Lee, Y.-S. Gao, Reciprocating Magnetorheological Polishing Method for Borosilicate Glass Surface Smoothness, J. Ind. Eng. Chem. 84 (2020) 243–251, https://doi.org/10.1016/j.jiec.2020.01.004.
[6] S. Sumitomo, H. Koizumi, M.A. Uddin, Y. Kato, Comparison of dispersion behavior of agglomerated particles in liquid between ultrasonic irradiation and mechanical stirring, Ultrason. Sonochem. 40 (2018) 822–831, https://doi.org/10.1016/j.ultsonch.2017.08.023.
[7] M. Vinatoru, T.J. Mason, I. Calinescu, Ultrasonically assisted extraction (UAE) and microwave assisted extraction (MAE) of functional compounds from plant materials, Trac-Trend. Anal. Chem. 97 (2017) 159–178, https://doi.org/10.1016/j.trac.2017.09.002.
[8] K. Su, J. Wu, D. Xia, Classification of regimes determining ultrasonic cavitation erosion in solid particle suspensions, Ultrason. Sonochem. 68 (2020) 105214, https://doi.org/10.1016/j.ultsonch.2020.105214.
[9] L. Rayleigh, On the pressure developed in a liquid during the collapse of a spherical cavity, Phil. Mag. 34 (1917) 94–98, https://doi.org/10.1080/14786440808635681.
[10] M.S. Plesset, A. Prosperetti, Bubble dynamics and cavitation, Annu. Rev. Fluid Mech. 9 (1) (1977) 145–185, https://doi.org/10.1146/annurev.fl.09.010177.001045.
[11] M. Mahdi R. Ebrahimi M. Shams Numerical analysis of the effects of radiation heat transfer and ionization energy loss on the cavitation Bubble´s dynamics Phys. Lett. A. 375 2011 /10.1016/j.physleta.2011.04.026. 2348 2361 https://doi.org.
[12] S. Behnia, A.J. Sojahrood, W. Soltanpoor, L. Sarkhosh, Towards classification of the bifurcation structure of a spherical cavitation bubble, Ultrasonics 49 (8) (2009) 605–610, https://doi.org/10.1016/j.ultras.2009.05.005.
[13] H.G. Flynn 57 6 1975 1379 1396.
[14] A. Aliabadi, A. Taklifi, The effect of magnetic field on dynamics of gas bubbles in visco-elastic fluids, Appl. Math. Model. 36 (6) (2012) 2567–2577, https://doi.org/10.1016/j.apm.2011.09.040.
[15] B. Saint-Michel, V. Garbin, Bubble dynamics for broadband microrheology of complex fluids, Curr. Opin. Colloid In. 50 (2020) 101392, https://doi.org/10.1016/j.cocis.2020.101392.
[16] C. Guo, X.J. Zhu, Effect of ultrasound on dynamics characteristic of the cavitation bubble in grinding flfluids during honing process, Ultrasonics 84 (2018) 13–24, https://doi.org/10.1016/j.ultras.2017.09.016.
[17] S. Zeng, X.M. Du, Theoretical analysis and experimental research of non-cavitation noise on underwater counter-rotation propellers, Prog. Comput. Fluid Dy. 20 (2020) 51–58, https://doi.org/10.1504/PCFD.2019. 10021373.
[18] T.C. Polachini, A. Mulet, J. Telis-Romero, J.A. Cárcel, Acoustic field of acid suspensions containing cassava bagasse: Influence of physical properties on acoustic attenuation, Appl. Acoust. 177 (2021), 107922, https://doi.org/10.1016/j.apacoust.2021.107922.
[19] K. Saraswathamma, S. Jha, P. Venkateswara Rao, Rheological behaviour of Magnetorheological polishing fluid for Si polishing, Mater. Today 4 (2) (2017) 1478–1491, https://doi.org/10.1016/j.matpr.2017.01.170.
[20] Y.Z.G. Man, F.J. Trujillo, A new pressure formulation for gas-compressibility dampening in bubble dynamics models, Ultrason. Sonochem. 32 (2016) 247–257, https://doi.org/10.1016/j.ultsonch.2016.03.013.
[21] S.J. Ruuth, S. Putterman, B. Merriman, Molecular dynamics simulation of the response of a gas to a spherical piston: Implications for sonoluminescence, Phys. Rev. E 66 (2002), 036310, https://doi.org/10.1103/PhysRevE. 66.036310.
[22] A. Bass, S.J. Ruuth, C. Camara, B. Merriman, S. Putterman, Molecular dynamics of extreme mass segregation in a rapidly collapsing bubble, Phys. Rev. Lett. 101 (2008):234301. https://doi.org/10.1103/ PhysRevLett.101.234301.
[23] E. Goncalvès, B. Charrière, Modelling for isothermal cavitation with a four-equation model, Int. J. Multiphase Flow 59 (2014) 54–72, https://doi.org/10.1016/j.ijmultiphaseflow.2013.10.015.
[24] A. Peters, H. Sagar, U. Lantermann, O. el Moctar, Numerical modelling and prediction of cavitation erosion, Wear 338-339 (2015) 189–201, https://doi.org/10.1016/j.wear.2015.06.009.
[25] A. Einstein, Eine neue Bestimmung der Molekuldimensionen. Ann. Phys. 19(1906) 289-306. https://doi.org /10.3929/ethz-a-000565688.
[26] V. Vand, Viscosity of solutions and suspensions, J. Phys. Coll. Chem. 52 (1948) 277, https://doi.org/10.1021/j150458a002.
[27] L. Ye, X. Zhu, Y. Liu, Numerical study on dual-frequency ultrasonic enhancing cavitation effect based on bubble dynamic evolution, Ultrason. Sonochem. 59 (2019), 104744, https://doi.org/10.1016/j.ultsonch. 2019.104744.

[28] Y.S. Liou, X.J. Kang, W.H. Tien, Particle aggregation and flow patterns induced by ultrasonic standing wave and acoustic streaming: an experimental study by PIV and PTV, Exp. Therm. Fluid Sci. 106 (2019) 78–86, https://doi.org/10.1016/j.expthermflusci.2019.04.011.
[29] B.M. Borkent, M. Arora, C. Ohl, N. De Jong, M. Versluis, D. Lohse, K.A. Mørch, E. Klaseboer, B.C. Khoo, The acceleration of solid particles subjected to cavitation nucleation, J. Fluid Mech. 610 (2008) 157–182, https://doi.org/10.1017/S002211200800253X.
[30] F. Zhao, Q.Yan, D.Cheng, Numerical study on the desorption processes of oil droplets inside oil-contaminated sand under cavitation micro-jets, Ultrason. Sonochem. 78(2021)105745.https://doi.org/ 10.1016/j.ultsonch.2021.105745.
[31] L.Z. Ye X.J. Zhu X.M. Wei S.A. Wu Damage characteristics and surface description of near-wall materials subjected to ultrasonic cavitation Ultrason. Sonochem. 67 2020 /j.ultsonch.2020.105175. 105175 https://doi.org/10.1016.
[32] L. Ye, X. Zhu, Analysis of the effect of impact of near-wall acoustic bubble collapse micro-jet on Al 1060, Ultrason. Sonochem. 36 (2017) 507–516, https://doi.org/10.1016/j.ultsonch.2016.12.030.
[33] H.B. Cheng, J.M. Wang, Q.J. Zhang, N.M. Wereley, Preparation of composite magnetic particles and aqueous magnetorheological fluids, Smart Mater. Struct. 18 (2009), 085009, https://doi.org/10.1088/0964-1726 /18/8/085009.
[34] M. Ashtiani, S.H. Hashemabadi, An experimental study on the effect of fatty acid chain length on the magnetorheological fluid stabilization and rheological properties, Colloids Surfaces A 469 (2015) 29–35, https://doi.org/10.1016/j.colsurfa.2014.12.046.
[35] L.L. Vignoli, A.L.F. de Barros, R.C.A. Thomé, A.L.M.A. Nogueira, R.C. Paschoal, H. Rodrigues, Modeling the dynamics of single-bubble sonoluminescence, Eur. J. Phys. 34 (3) (2013) 679–688, https://doi.org/10.1088/0143-0807/34/3/679.
[36] I.D. Jun, M. Kim, S.J. Park, A comprehensive viscosity model for micro magnetic particle dispersed in silicone oil, J. Magn. Magn. Mater. 404 (2016) 40–44, https://doi.org/10.1016/j.jmmm.2015.12.024.
[37] H. Nazari-Mahroo, K. Pasandideh, H.A. Navid, R. Sadighi-Bonabi, How important is the liquid bulk viscosity effect on the dynamics of a single cavitation bubble? Ultrason. Sonochem. 49 (2018) 47–52, https://doi.org/10.1016/j.ultsonch.2018.07.013.
[38] J. Luo W. Xu Y.W. Zhai Qi. Zhang, Experimental study on the mesoscale causes of the influence of viscosity on material erosion in a cavitation field Ultrason. Sonochem. 59 2019 /10.1016/j.ultsonch.2019.104699. 104699 https://doi.org.
[39] X.F. Dong, N. M , M. Qi, et al., Properties of magneto-rheological fluids based on amorphous micro-particles, Trans. Nonferrous Met.Soc.China 22(2012)2979-2983. https://doi.org/10.1016/S1003-6326 (11)61559-8.
[40] J. Song, Q. Wang, Y. Zeng, Y. Liu, W. Jiang, Deposition of protein-coated multiwalled carbon nanotubes on oxide surfaces and the retention in a silicon micromodel, J. Hazard. Mater. 375 (2019) 107–114, https://doi.org/10.1016/j.jhazmat.2019.04.077.
[41] Z. Huang, M. Lin, R. Qiu, J. Zhu, J. Ruan, R. Qiu, A novel technology of recovering magnetic micro particles from spent lithium-ion batteries by ultrasonic dispersion and waterflow-magnetic separation, Rescources, Conservation&Recycling 164 (2021) 105172, https://doi.org/10.1016/j.resconrec.2020.105172.
[42] T. Prozorov, R. Prozorov, K.S. Suslick, High velocity interparticle collisions driven by ultrasound, J. Am. Chem Soc. 126 (43) (2004) 13890–13891, https://doi.org/10.1021/ja049493o10.1021/ja049493o.s001.
[43] H. Zarepour, S.H. Yeo, Predictive modeling of material removal modes in micro ultrasonic machining[J], Int. J. Mach. Tools & Manu. 62 (2012) 13–23, https://doi.org/10.1016/j.ijmachtools.2012.06.005.
[44] I. Bica, Y.D. Liu, H.J. Choi, Physical characteristics of magnetorheological suspensions and their applications, J. Ind. Eng. Chem. 19 (2) (2013) 394–406, https://doi.org/10.1016/j.jiec.2012.10.008.